Interaction of *Cassiopea* feeding and exchange currents with steady ambient flows

Manikantam G. Gaddam, Matthew Takyi-Micah, Naman Mathur and Arvind Santhanakrishnan*

School of Mechanical and Aerospace Engineering, Oklahoma State University, Stillwater, OK 74078, USA

*Author for correspondence (askrish@okstate.edu)

SUMMARY

A large number of marine benthic invertebrates capture prey using suspension feeding. Previous studies on bivalves, sponges, and crustaceans have shown the generation of steady currents that assist with the prey capture process. In contrast, the benthic upside-down jellyfish (*Cassiopea* spp.) uses unsteady bell pulsations to generate feeding and exchange currents while remaining attached to the substrate. This organism can serve as a useful model for examining how unsteady currents can aid suspension feeding in low-speed ambient flows seen in shallow marine environments. In this study, *Cassiopea* medusae with bell diameters ranging between 2 cm to 7 cm were investigated in a recirculating flow tank under background flows of 0.5 cm s^{-1} to 2 cm s^{-1} using videography and 2D particle image velocimetry (PIV) to quantify the bell kinematics and flow field characteristics. Time-resolved PIV (TR-PIV) measurements in the near-field of the medusae showed the formation of a starting vortex during power stroke and a counter-signed stopping vortex on the downstream side of the bell during the recovery stroke. Regardless of pulsation phase and background flow speed, continuous vertical jets were driven through the oral arms of the medusae at velocities on the order of 0.3 cm s^{-1}. At 2 cm s^{-1} background flow, vertical penetration depth of *Cassiopea*-induced jets showed an inverse relationship with bell diameter. Volumetric flux was calculated at x/d = -0.5, 0.5 and 1 with no background flow and with 2 cm s^{-1} background flow conditions to understand the flow entrainment along the medusa current. Finally, under background flows, flow structure with prey-sampled water decelerates due to the oral arms increasing the scope for prey retention time and ensuring the suspension feeding to occur.

Key words: upside-down jellyfish, *Cassiopea*, unsteady flow, Lagrangian coherent structures, suspension feeding

INTRODUCTION

A large number of sessile marine invertebrates such as sponges, gorgonians, brachiopods, polychaete tube worms, and bivalves use some form of suspension feeding. Previous studies on bivalves (Monismith and Koscf, 1990; O'Riordan et al., 1995) and sponges (Riisgård et al., 1993; Vogel, 1974), have characterized the steady currents generated by these organisms for suspension feeding. In addition to organism-induced currents, sessile invertebrates inhabiting the benthic boundary layer have to often interact with ambient flows that are continuous or oscillatory. Laboratory-level experiments show that prey capture rates can be increased in oscillating flows when compared to the continuous flow conditions (Hunter, 1989).

In addition to ambient flow conditions, many suspension feeders have flexible and/or branched feeding structures that bend and reconfigure under flow. Particle capture in colonies of flexible sessile hydrozoans has been observed to mostly depend on the background flow velocity, colony reorientation and fluid resampling (Hunter, 1989). Reduction of drag by reconfiguration of gorgonian colonies under steady background flow was shown to not be important in preventing dislodgement, but reduced flow velocities around polyps and enabled higher feeding efficiencies under high ambient velocities (Sponaugle and LaBarbera 1991). The flow velocity over a colony of flexible suspension feeders was observed to be dampened to increase the time scale available for suspension feeding (Ferner and Gaylord, 2008). A common theme observed from these studies is the conflicting need for drag reduction for preventing dislodgement from the substrate, while maximizing surface area to enhance food capture and exchange. Examining the diverse range of suspension feeding strategies used by sessile, benthic invertebrates could help in improving our understanding as to whether the choices of: (a) active (e.g., sponges) versus passive (e.g., gorgonians) feeding mechanisms; and (b) flexible, non-branched versus flexible, branched feeding appendages, have an ecological underpinning based on the specific environmental flow conditions. In contrast to the above studies, active suspension feeding by sessile benthic invertebrates that generate unsteady currents has received comparatively limited attention. It can be expected that the physical mechanisms underlying active suspension feeding using unsteady jets would differ from sessile invertebrates that either generate continuous jets (e.g., sponges) or feed in unsteady ambient flows (e.g., sea anemones). We use the benthic *Cassiopea* jellyfish as a model organism in this study to examine how unsteady currents generated by their bell pulsations can impact suspension feeding in low-speed, steady ambient flows.

Cassiopea medusae, also known as "upside-down jellyfish", are found in patchy aggregations (Templeman and Kingsford, 2010; Niggl and Wild, 2010) in the benthic boundary layer of shallow, coastal environments such as mangrove swamps, coral reefs, and seagrass meadows. The various habitats of *Cassiopea* are typically characterized by low-speed ambient flows on the order of 1 cm s^{-1} or lower (Arai, 2001; Maze et al., 2007, LaBarbera, 1984; Santhanakrishnan et al., 2012). Population densities of 31 individuals m^{-2} have been observed in *Cassiopea* aggregations (Todda et al., 2006). The morphology of *Cassiopea* includes an oblate bell with eight frilled, cylindrical oral arms containing numerous frilly branches (secondary mouths) fused over a central mouth (Brusca and Brusca, 2003). These organisms exhibit a sessile lifestyle, with their bell attached to the substrate and oral arms pointing towards the sunlight (Arai, 1997). *Cassiopea* individuals rhythmically contract and expand their bell margins, entraining water adjacent to the substrate and generating vertical currents by directing the sampled water through their oral arms for suspension feeding. These organism-induced vertical currents have been proposed to minimize

recirculation of previously sampled water volume, while also providing the suction force necessary for the medusa to prevent dislodgement from the substrate (Santhanakrishnan et al., 2012).

Time-resolved and phase-averaged particle image velocimetry (PIV) measurements on *Cassiopea* individuals under no background flow have shown the formation of a starting vortex near the bell margin during the power stroke (bell expansion to contraction) of pulsations, with peak velocities on the order of 10 cm s^{-1} (Santhanakrishnan et al., 2012). Kinematics analyses showed an increase in fineness ratio (bell height to bell diameter) during the power stroke and decrease in fineness ratio during the recovery stroke (Santhanakrishnan et al., 2012). During *Cassiopea* bell pulsations in an initially quiescent medium, ambient water was entrained towards the medusa and then it was passed through the sieve formed by the oral arm network. A numerical study examining the currents generated by *Cassiopea* spp. under no background flow conditions showed that the presence of oral arms increased the volumetric flux (Hamlet et al., 2011). Additional numerical studies on this organism with background flow were conducted to understand its prey capture mechanism (Hamlet et al., 2012). Overall, these studies suggest that the oral arms play an important role in suspension feeding, by trapping the vortices formed during the pulsations and increasing prey retention time (Hamlet et al., 2011; Santhanakrishnan et al., 2012; Hamlet et al., 2012). However, the numerical models used in the above studies were limited to 2D representation of the bell pulsations. This modeling simplification was attributed as one of the reasons for disagreement of the simulations with the experimental PIV measurements on *Cassiopea* individuals in terms of the far-field flow above the medusa (Santhanakrishnan et al., 2012). Further, the oral arms were modeled as a homogeneous porous layer in the numerical models. Finally, though the natural environment of *Cassiopea* is characterized by low–speed background flows on the order of 1 cm s^{-1} (Santhanakrishnan et al., 2012), the interactions of organism-induced currents with non-zero background flows have not been previously examined in live medusae.

In this study, we examined the hydrodynamic interactions of *Cassiopea* bell pulsation-induced currents with steady ambient flows to understand how medusae of varying bell diameter could alter their unsteady currents to slow down the flow in the vicinity of their oral arms. The medusae were tested in a recirculating laboratory flow tank under varying steady background flows ranging from 0-2 cm s^{-1}. 2D videos were used to quantify bell pulsation kinematics. 2D time-resolved PIV measurements were obtained to visualize the formation of flow structures near the bell margin and interactions with background flow. 2D time-averaged PIV measurements were used to quantify bulk flow characteristics of variable medusa size on background flow and implications for suspension feeding.

MATERIALS AND METHODS

Cassiopea spp. collection and handling

Cassiopea individuals of varying bell sizes were obtained from Carolina Biological Supply, NC, USA, during May 2016. Five individuals were used in this study with bell diameters ranging from 2 cm to 7 cm. The medusae were transported overnight and placed in a 20-gallon glass aquarium maintained at 20-24ºC with artificial salt water with salinity of 1.024 g L^{-1}. The medusae were target fed with live *Artemia* spp. nauplii for every two days. Metal halide lighting was used in a 20-gallon housing tank, and it was set to operate between 8-10 hours continuously on a daily basis. Submersible heaters were used to ensure the housing tank water was maintained at a temperature range of 20-24ºC. All the experiments were conducted at room temperature during summer of 2016 (May to July).

Low-speed recirculating flow tank

Fig. 1 represents the recirculating flow tank that was designed in the same manner as outlined by Vogel and LaBarbera (Vogel, 1978; LaBarbera, 1984). The entire test section, measuring 0.3 m x 0.3 m (1 ft x 1 ft) in cross-section, was fabricated from 0.03 m (1 inch) thick acrylic sheets for optical access. Custom flow straighteners were inserted near the entrance and exit of the test section to generate uniform flow across the observation window used in this study. The section between the two flow straighteners (where medusae were placed for testing) measured 0.3 m x 0.3 m (1 ft x 1 ft) in cross-section and 0.9 m (3 ft) in length. Flows with mean velocities in the range of 0 - 2 cm s^{-1} were produced for this study via a universal DC motor **(**1/3 hp, 1800 rpm, AutomationDirect**,** GA, USA) regulated with a variable speed DC controller with 50:1 speed reduction (Dart Controls, Inc., IN, USA). A custom gearbox with 250:1 speed reduction and two 10:1 pulleys, both fabricated via 3D printing, were connected via commercial timing belts to the DC motor shaft for the multiple orders of magnitude speed reduction needed for obtaining the above ambient flow speed range. The DC motor drove a 3D printed, 3-bladed propeller (with fixed stator blades) that was positioned vertically inside the return piping following the test section exit. Rotation of the propeller drove the flow unidirectionally through the test section. A sand bed was made using a commercially available black substrate (CaribSea Instant Aquarium Tahitian Moon Reef & Marine Substrate, CaribSea Inc., FL, USA) with 0.1-0.3 mm grain diameter. A substrate depth of 0.05 m (2 inches) was used for qualitative flow visualization tests, while a substrate depth of 0.03 m (1-inch) was used for all PIV measurements. Artificial saltwater with salinity of 1.025 g/L was made from 150-gallons of deionized water using commercial aquarium sea salt (Instant Ocean Spectrum Brands, VA, USA) and used to fill the recirculating flow tank.

Bell kinematics

Bell kinematics experiments were conducted on *Cassiopea* individuals placed inside a 3-gallon cubic plastic aquarium with dimensions of 12.7 cm x 12. 7 cm x 12 cm. Video recordings were obtained using a digital camera (EOS70D, Canon Inc., Japan) with a maximum spatial resolution of 1,920 x 1,080 pixels. All videos for bell kinematics analyses were acquired using 60 mm focal lens at a frame rate of 30 Hz. A dark background and black substrate were used to provide additional contrast between the medusa and its surroundings. Each medusa was moved into the tank after verifying the water conditions were closely matched to the 20-gallon aquarium used for housing the animals. The following conditions were matched between the test and housing aquaria: pH, salinity, temperature, ammonia, nitrate, and nitrite. Each medusa was drip-acclimated into the test aquarium and a half-day resting period was provided for every individual to settle on the substrate. After 12 hours, a plastic ruler was placed above the substrate, bisecting the central plane of medusa bell and perpendicular to the camera image. The camera was focused to obtain nearly uniform illumination across the image planes. A still image of the ruler was acquired for scaling from pixels to cm. The experimental recordings consisted of a minimum 10 continuous bell pulsation cycles. The recorded images were digitized and processed using MATLAB DLTdv5 program (Hedrick, 2008). Eight points were digitally selected on one side of bell margin, and one point on the oral arm (**Fig. 2**) and these points were tracked manually across 10 continuous pulsing cycles. Bell fineness ratio F_i, defined as the ratio of bell height h to average bell diameter d, and arm fineness ratio, defined as the ratio of arm tip height to average bell diameter, were obtained from the digitized images. Eight points on bell were used to quantify bell motion and one point on the oral arm was used to examine its movement concerning the bell. Reference points were placed only on half of the bell diameter assuming radial symmetry and were investigated.

Qualitative flow visualization

A single, *Cassiopea* individual with bell diameter d = 4 cm was placed in the recirculating flow tank with a sand bed of 2-inch height, after verifying the water conditions with the main tank; including salinity, temperature and the previously mentioned chemical conditions. 5 ml of organic red food color (McCormick & Co., Inc., MD, USA) was added to 1 L of de-ionized water and was filled into a micro-pipette. The micro-pipette tip was positioned just above the substrate adjacent to the medusa, in the upstream position (approximately 2d to the left of the medusa, observed in the camera view), such that ejected dye would flow along the central plane of the organism (**Fig 3**). The dye was injected into the water when the medusa started pulsing, for visualizing the flow structures generated by the interaction of pulsation-induced currents with the background flow. For these tests, background flow ranging from 0 - 2 cm s^{-1} was used. Videos were recorded using at a frame rate of 30 Hz using the same camera used for bell kinematics measurements (EOS70D, Canon Inc., Japan).

2D Time-resolved particle image velocimetry (PIV)

Experimental setup for PIV is shown in **Fig. 4**. 2D time-resolved PIV was performed on an individual medusa with 2 cm bell diameter. High-speed videos were recorded with 1 megapixel CMOS camera (Phantom Miro 110, Vision Research Inc., Wayne, NJ, USA) at a frame rate of 696 Hz using a 60mm constant focal length lens (Nikon Micro Nikkor, Nikon Corporation, Tokyo, Japan). The maximum spatial resolution of the camera (1280 x 800 pixels) was used for recording. Two background flows of mean velocities 0.45 cm s^{-1} and 2 cm s^{-1} were considered for this set of experiments. The field-of-view (FOV) used was ± 1.5 d measured from the center of the medusa. The flow field was illuminated using a 0.5 mm diameter beam outputted by a 35mJ high-speed, single cavity Nd:YLF laser (Photonics Industry Inc., NY, USA) with wavelength 527 nm. The beam was converted into a planar sheet of 3 mm thickness using a cylindrical lens (focal length = 20 mm). The laser sheet was positioned to be perpendicular to the substrate along the diameter of medusa as shown in **Fig. 4.** Hollow glass spheres of 8 – 10 μm diameter (LaVision GmbH, Gottingen, Germany) were used as seeding particles. Small amounts of these seeding particles were mixed in with water from the flow tank in a 1000 mL beaker before being added into the tank. This process was repeated with the water recirculating until uniform particle seeding density in the range of 10-20 particles for 5-10 pixels/particle was obtained and particle displacements in the range of 4-7 pixels were measured between two successive images. Both the Nd: YLF laser and the camera were connected to the high-speed controller. This controller was then connected to a central computer that was used for image acquisition. The recordings used for this study did not commence until after the flow tank was continuously operating for at least 1-hour, to allow time for uniformly mixing the seeding particles and also to provide a short period for the medusa to adjust to their new environment.

For each 2D time-resolved PIV run, 100 images were acquired to obtain atleast one complete pulsation (both power stroke and the recovery stroke). Five test runs for each medusa for all background flows were recorded to obtain five complete pulsing cycles and processed to obtain 2D velocity vector fields. The raw images were processed using multi-pass cross-correlation in DaVIS 8.2.0 software (LaVision GmbH, Gottingen, Germany). The interrogation window sizes used were 96 x 96 pixels with 50% overlap (2 passes) and 48 x 48 pixels with 50% overlap (2 passes). Post-processing was performed by rejecting velocity vectors with a peak ratio of less than 1.2 and interpolating the empty vectors. The processed data were exported into ".dat" file format, where each file consisted of spatial coordinates (x, y) and corresponding 2D velocity components (horizontal component u in the x-direction and vertical component v in the y-direction). Velocity fields corresponding to each phase percentage in all test runs were exported as ".dat" files and were then phase-averaged using MATLAB (The Mathworks, Inc., Natick, MA) program to get

single .dat file containing vertical co-ordinate y, horizontal co-ordinate x, vertical velocity component v, horizontal velocity component u, and 2D velocity magnitude V. This .dat file was then processed in TecPlot360 (Tecplot Inc., WA, USA) to get time-resolved 2D PIV results.

2D Time-averaged PIV

2D time-averaged PIV measurements were conducted to quantify bulk flow characteristics across multiple medusae of different sizes under varying background flows. Experimental setup used was the same as that of 2D time-resolved PIV, except that images were acquired using a sCMOS camera (LaVision GmbH, Gottingen, Germany) with full resolution of 2600 x 2200 pixels in double-frame mode. Laser pulse separation times (time between two images in an image pair) ranged from 10-20 ms, depending on the magnitude of background flow. The frame rate of 15 Hz was used for time-averaged PIV recordings, with a field of view of ± 1.5 d. Particle displacements between two images in an image pair were ensured to not exceed 25% of the smallest interrogation window size (8 pixels). Fourteen pulsation cycles under each background flow were recorded and processed using multi-pass cross-correlation in DaVIS 8.2.0 software (LaVision GmbH, Gottingen, Germany). The interrogation window sizes included 64 x 64 pixels with 50% overlap and 32 x 32 with 50% overlap (2 passes each). Post-processing was performed by rejecting velocity vectors with a peak ratio of less than 1.2 and interpolating the empty vectors. Following post-processing, time averaging was performed in DaVIS 8.2.0 software to result in a single 2D velocity vector field. The time-averaged image was exported in .dat file format containing 2D spatial coordinates (x, y) and 2D velocity components (horizontal component u and vertical component v) and imported to TecPlot360 (Tecplot Inc., WA, USA) for extracting velocity profiles. LCS MATLAB kit version 2.3 (developed in Biological Propulsion Laboratory at California Institute of Technology using definition of Shadden et al., 2005) was used to process 2D time series velocity fields to compute corresponding finite time Lyapunov exponent fields (FTLE). These FTLE fields were used to identify Lagrange Coherent Structures (LCS) such as vortex and other fluid barriers. A custom program, written in MATLAB (The Mathworks, Inc., Natick, MA), was used to calculate volumetric flux upstream and downstream of the medusa.

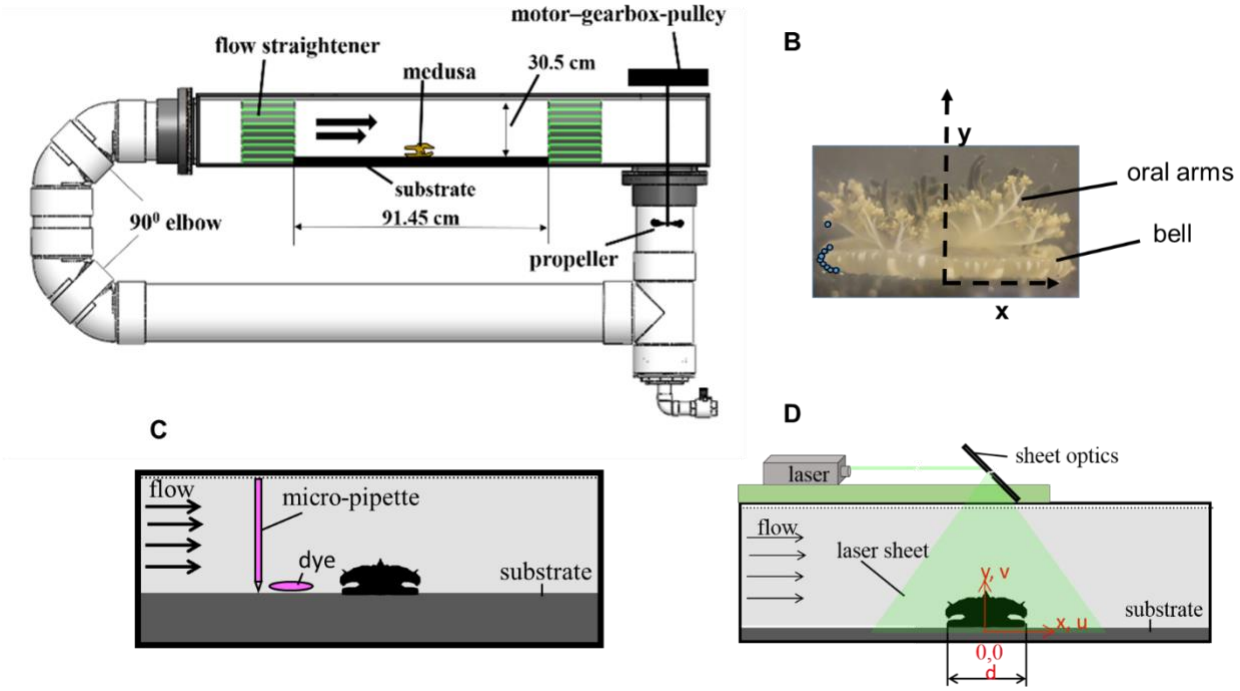

Figure 1. A) Schematic diagram (not to scale) of recirculating flow tank used to introduce background flows on Cassiopea individuals. The medusa was positioned in between two flow straighteners as shown. Individual animals were placed on top of the sand bed. B) Representative image of bell kinematics with eight markers on bell margin and a single marker on the distal end of the oral arm. Flow visualization experimental setup. The coordinate system origin was defined at the center of medusa. C) Dye was fed from a micro-pipette adjacent to the substrate of 2 in depth and upstream of the medusa. D) Experimental setup used for 2D PIV measurements (time-resolved and time-averaged). Horizontal velocity component (u) is defined along the x-axis, vertical velocity component (v) is defined along y-axis and d is bell diameter in mm.

RESULTS

Bell kinematics

Temporal patterns of bell pulsations were manually analyzed from the recorded frames to evaluate durations of the power stroke, recovery stroke, and the complete cycle. Each cycle was divided into two parts of 0% to 100%, with 20% increment, consisting of the power stroke and recovery stroke frame number. Power stroke time and recovery stroke time for each cycle for an individual *Cassiopea* was calculated by the difference of 0% and 100% divided by the recording frame rate of 30 frames s^{-1}. **Fig. 5** shows the pulsing frequency variations across the individual medusae used in the experiments and across all background flows (0 cm s^{-1}, 0.5 cm s^{-1} and 2 cm s^{-1}). Pulsing frequency increased for bell diameter d =3 cm from d= 2 cm and later it decreased with increase in bell diameters from 4 cm through 7 cm. The standard deviation was calculated based on variable background flow for each medusa.

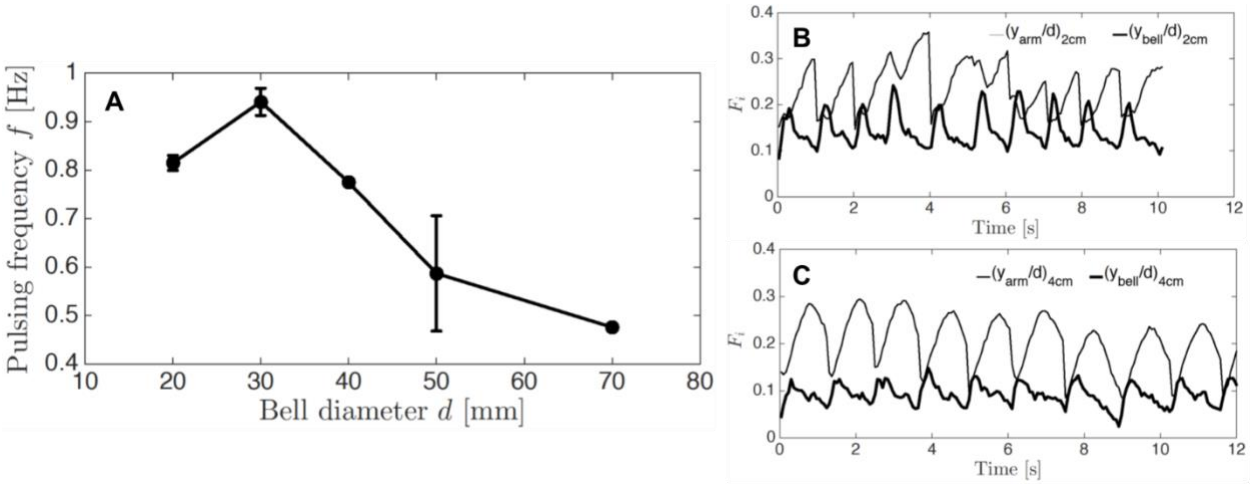

Figure 2A) The plot shows variations of pulsing frequency with standard deviations for each medusa under variable background flows (0 cm s^{-1}, 0.5 cm s^{-1} and 2 cm s^{-1}).B) Fineness ratio vs. time. Bell fineness ratio and arm fineness ratio was plotted against time for medusa with bell diameter d = 2 cm (plot B) and d = 4 cm (plot C) for 10 pulsing cycles. The plot shows the increase in fineness ratio during the power stroke and decrease in fineness ratio during the recovery stroke for both medusae. Also, the fineness ratio of bell and arm are appeared to be phase shifted by 180 degrees.

The fineness ratio (F_i) for the bell and the arm were analyzed for *Cassiopea* individuals with bell diameters of 2 cm and 4 cm respectively. Bell motion was inward (towards the center) during the power stroke. During the recovery stroke, the bell moved outwards and downward towards the substrate.

The bell kinematics conducted on the two different size medusae were observed under no background flow. The kinematics result is shown in **Fig. 6A** and **Fig. 6B** are in agreement with previous observations (Santhanakrishnan et al., 2012) such that during the contraction phase, the bell tip height increased, increasing the bell fineness ratio. During the recovery stroke, the bell tip height decreased, and the bell fineness ratio decreased. In contrast, the arm fineness ratio for both medusae increased during the recovery stroke and followed by a sharp decrease in fineness ratio during the power stroke. Both 2 cm and 4 cm individuals had longer oral arms compared to their bell diameters, and therefore, their respective plots show the arms overlapping the bell as shown in **Fig. 6A and Fig. 6B** respectively.

Qualitative flow visualization

Under no background flow conditions (**Fig 7a-e**), colored dye released from the micro-pipette was entrained into the subumbrellar cavity of the medusa during the contraction phase of bell pulsation as shown in **Fig 7a-c**. This resulted in the formation of a starting vortex adjacent to bell margin which was directed toward the oral arms during the recovery stroke (**Fig 7d and 7e**). The elaborate network of the oral arms provides resistance to the flow, breaking up the coherent starting vortex into small-scale flow structures. These small-scale flow structures were introduced into the water column in the form of a vertical jet as shown in **Fig. 7d** and **7e**. The change in dye coloration near the substrate and above the oral arms suggests that the oral arms diffused the dye by slowing down the jet. A similar observation was found under background flow of 0.5 cm s^{-1} (**Fig 7f-7j**) and 2 cm s^{-1} (**Fig 7k-7o**) as shown. The small-scale flow structures were less diffuse under non-zero background flow as shown in the second and third column. For more information, look at the supplementary movies (**Movie S1- S3**).

Figure 3. Qualitative flow visualization of *Cassiopea* currents. Each column shows the progression of one pulsing cycle (time period of T) at various time points for bell diameter 9 cm under no background flow conditions (left column), 0.5 cm/s in the middle column, and 2 cm/s condition in the right column. While the first row is the start of the power stroke. The second row gives information about starting of flow structure. The third row shows the end of the power stroke. Fourth and fifth rows show information of 50% recovery stroke and 100% recovery stroke respectively.

Time-resolved flow characteristics

Power stroke

Phase-averaged velocity vector fields were examined for a 2 cm medusa under background flows of 0.5 cm s^{-1} and 2 cm s^{-1}. **Fig. 8** shows the flow fields at specific instances of power stroke for 2 cm medusa under 0.5 cm s^{-1} background flow. At 20% PS, the water around the individual was pulled towards bell margin along the substrate with 0.3 cm s^{-1} as shown in **Fig. 8A**. At 60% PS starting vortex formation was observed, and fluid velocity at bell margin was increased to 0.6 cm s^{-1} as shown in **Fig. 8B**. Further, into the pulsing cycle, this vortex was carried along the bell margin and was directed vertically through the oral arms. The velocity of current induced into background flow was around 0.35 cm s^{-1}. The leading vortex (upstream end of bell margin) formed was smaller compared to the trailing vortex (downstream end of bell margin), due to diminishing influence of background flow with increasing downstream distance.

A similar pattern was observed in power stroke of the same 2 cm individual when background flow was increased to 2 cm s^{-1} as shown in **Fig. 9A-C**. When the background flow increased the vortex with velocity vectors of 0.5 cm s^{-1} in downstream bell margin location was observed while a smaller vortex formation was observed in upstream bell margin point as shown in **Fig. 9C**. This was due to the interaction of the background flow on the vortex structure.

Recovery Stroke

On observation of recovery stroke vector field time-resolved images, the vortex was advected upward at 20% RS as shown in **Fig. 8D**. This vortex diminished as the recovery stroke progress. At 60% RS, water started to expel out with 0.3 cm s^{-1} into upstream and 0.4 cm s^{-1} in downstream as shown in **Fig. 8E**. The water present inside sub-umbrella region was appeared to expel out as recovery stroke progressed. At the end of recovery stroke, 100% RS, no significant water movement was observed in the downstream direction, as shown in **Fig. 8F**.

As the background flow increased to 2 cm s^{-1}, the velocity vectors in vortex decreased in the upstream side during 20% RS as shown in **Fig. 9D** while the velocity value was approximately same in the downstream side. Vortex was advected into the water column, and velocity vectors in vortex were approximately 0.3 cm s^{-1}. As recovery stroke progressed, on downstream of medusa water started to expel out as shown in **Fig. 9E**. At the end of 100% RS, no flow was observed on downstream but flow structure similar to vortex was observed on upstream near bell margin as shown in **Fig. 9F**. Asymmetry in vortices advection was observed due to increased background flow.

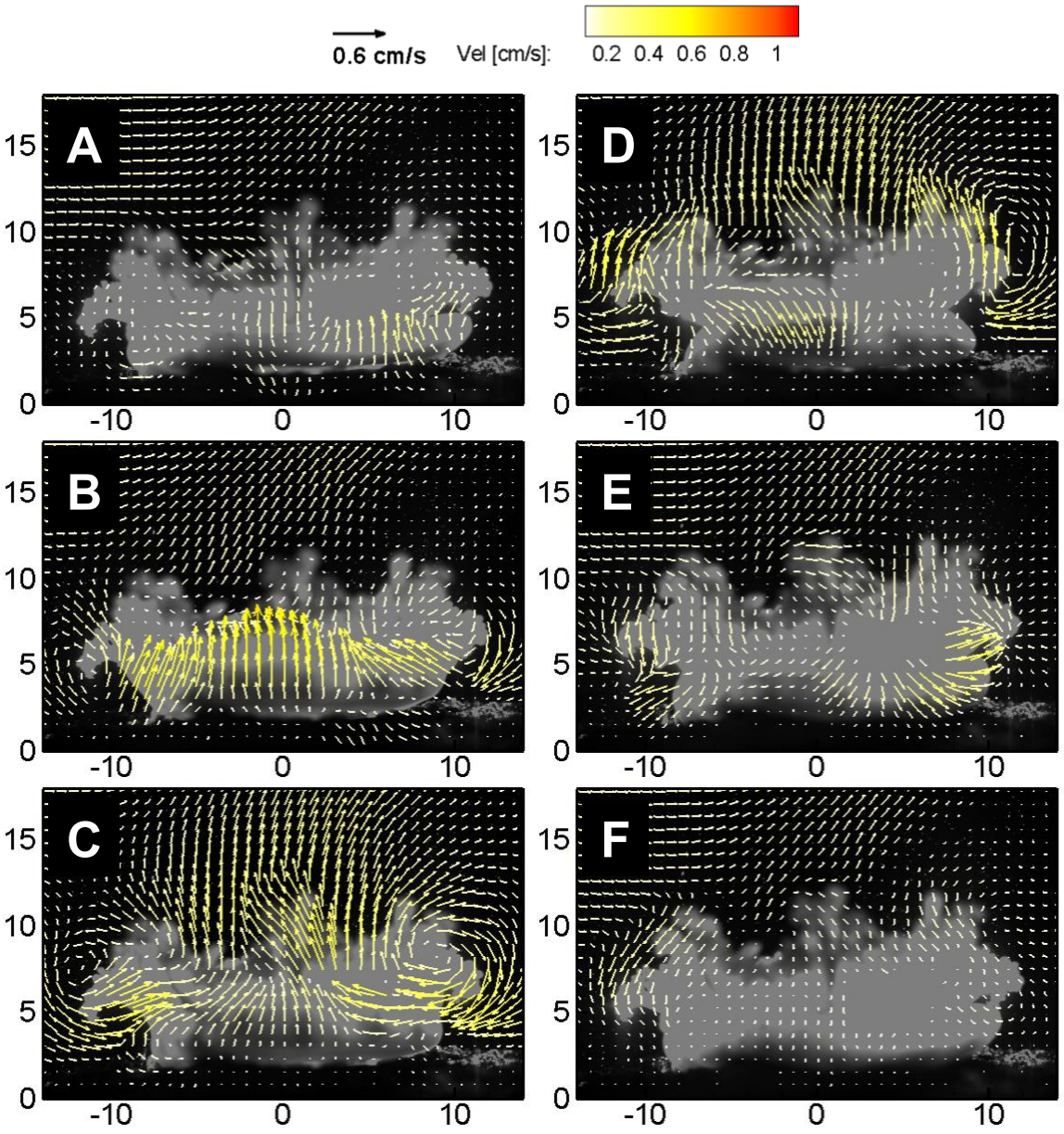

Figure 4. Time-resolved velocity vector field images of 2 cm *Cassiopea* medusa with background flow of 0.5 cm s^{-1}. (A)20% of power stroke, (B) 60% of the power stroke, (C) 100% of the power stroke, (D) 20% of recovery stroke, (E) 60% of recovery stoke and (F) 100% of recovery stroke. Length of vectors represents their magnitude as shown in legend and arrowhead indicates the flow direction.

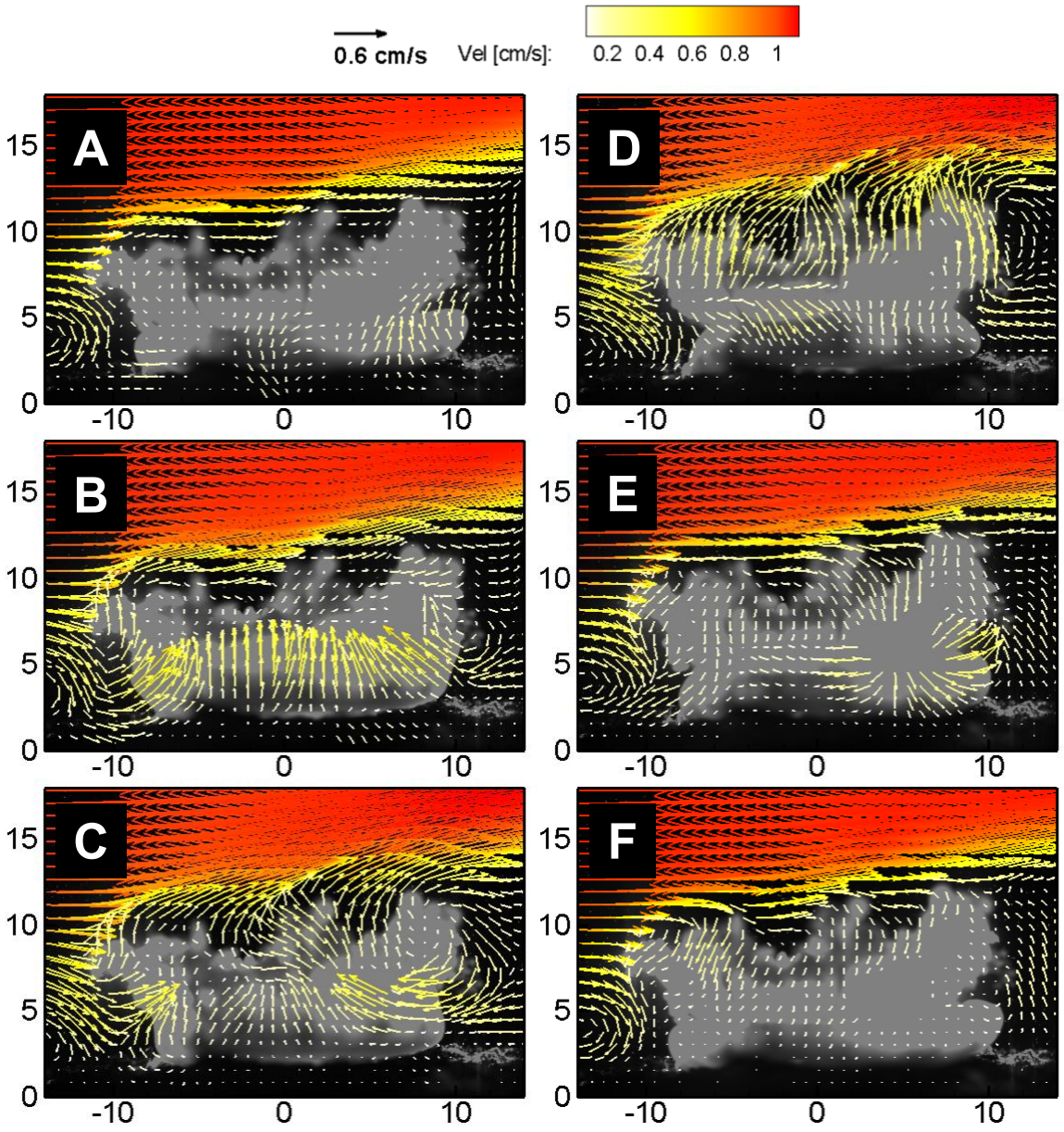

Figure 5.Time-resolved velocity vector field images of 2 cm *Cassiopea* medusa with background flow of 2 cm s^{-1}. (A) 20% of power stroke 20%, (B) 60% of the power stroke, (C) 100% of the power stroke, (D) 20% of recovery stroke, (E) 60% of recovery stoke and (F) 100% of recovery stroke. Length of vectors represents their magnitude and arrowhead indicates the flow direction.

Lagrangian coherent structures (LCS)

LCS were identified using finite-time Lyapunov exponent (FTLE) to characterize medusa jet characteristics in entrainment, detrainment and mixing of flow structures in no background flow (**Fig 6a**) and with background flow condition (**Fig 6b**). In no background flow, an entrainment lobe was observed with maximum FTLE value, indicating the fate of nearby particles over finite time interval i.e, 20% power stroke (**Fig 6a-i**) . This entrainment lobe was observed vertically for few mm, and increased its size showing more chances for particle trap in the form of vortex structure near the bell as seen at 60% PS in (**Fig 6a-ii**). This entrainment lobe region was narrowed as time progress to 100% PS (**Fig 6a-iii**) and decreased the chances for prey capture compared with 60% PS. This entrainment lobe was pushed into water column above oral arms with progression of recovery cycle 20%RS (**Fig 6a-iv**). A narrow LCS was observed at the bell tip in recovery structure, due to stopping vortex at the 20% RS and continued up to 60% RS (**Fig 6a-v**). A continuous flow mixing Lagrange coherent structure was observed above oral arms location due to the interaction of flow structures produced during power stroke of a pulsing cycle.

As background flow increased to 2 cm s^{-1} (**Fig 6b**) the entrainment lobe on upstream of medusa increased its size during PS (**Fig 6b-i-iii**), increasing chances for more prey encapsulation. Upstream of medusa showed an increase in prey entrainment due to added benefit of inflow water into bell region. In the background flow of 2 cm s^{-1}, entrainment lobe was found to be of same size with same FTLE value at the bell tip in the downstream due to decelerated zone. Medusa current was significantly influenced by background flow as LCS lobes were angled towards the downstream direction. However, the LCS region on the downstream of medusa remained to display the same particle fate in background flow, due to the influence of medusa jet shearing into background flow causing a decelerated zone in the downstream.

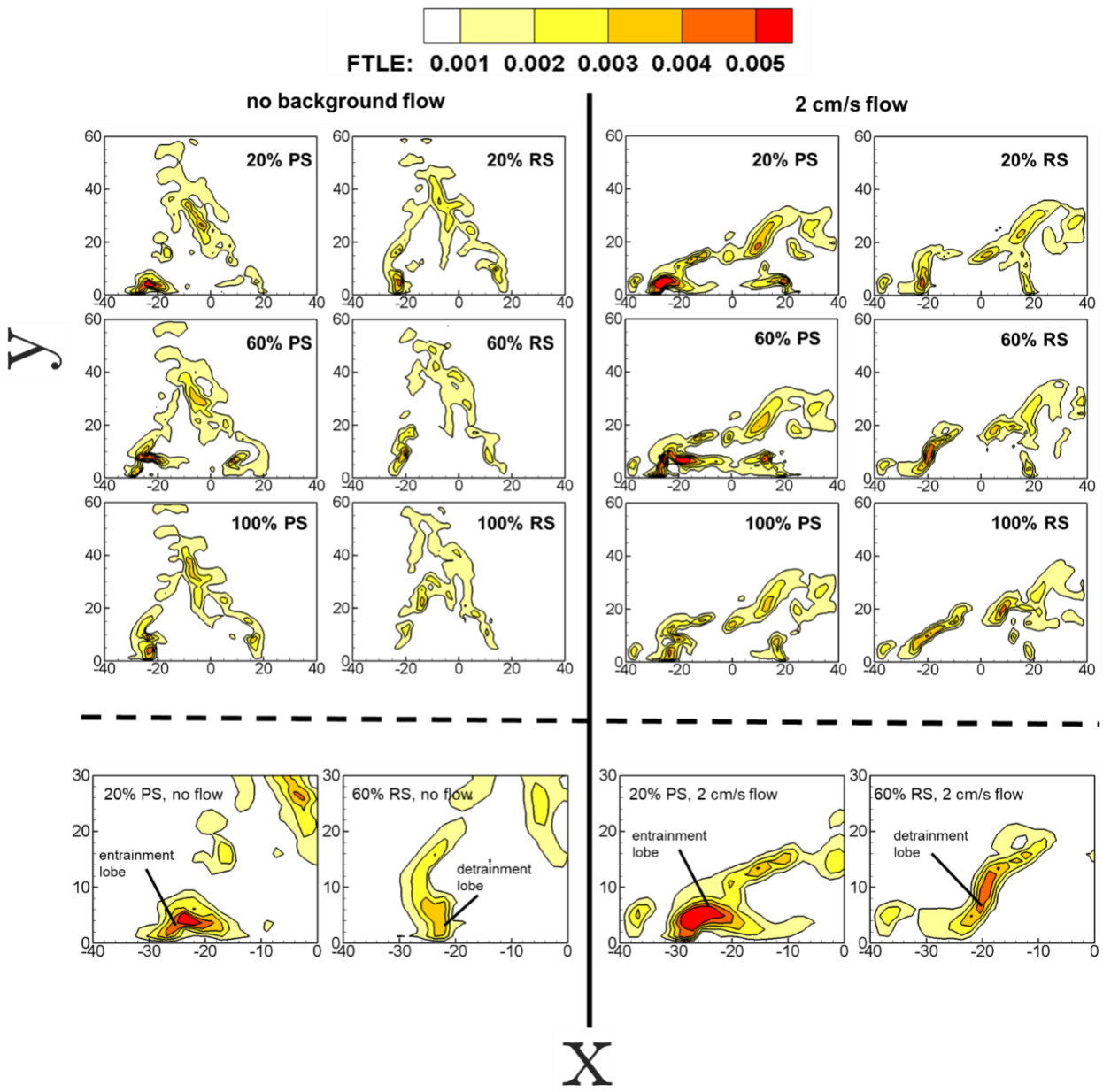

355

356 Figure 6. Time resolved Lagrangian Coherent structures of Cassiopea medusa of bell diameter d = 2 cm in no
357 background flow and with background flow. Bottom insert shows the zoomed figures of 20% PS and 60% RS in no
358 background flow condition and with background flow of 2 cm s^{-1}.

359

360

361 **Cycle-averaged flow characteristics**

362 **Velocity profiles**

To look at the depth of medusa jet penetration, vertical velocity profiles were plotted at different background flow conditions as shown in **Fig 7(I)**. These plots show that under no background flow (solid markers), the velocity reach peak value at y/d = 1.75 along the center of 2 cm medusa. In background flow of 2 cm/s (open markers), the velocity peaked at y/d =1.25 and x= 20 mm. This indicates that the medusa jet has the capability to penetrate at least 1.25 times its diameter in presence of background flow of up to 2 cm s^{-1}.

To understand this jet penetration, horizontal velocity profiles were plotted as shown in **Fig. 7(II)**. For a particular medusa, as the background flow increases from 0 cm s^{-1} to 2 cm s^{-1}, the horizontal velocity component u at various locations along substrate were plotted against the vertical column height as shown in **Fig. 7(II)**. The decrease in horizontal velocity component u can be observed at x = d and 1.5 d. This decrease in horizontal component u was due to the interaction of medusa jet with the background flow. Also, the interaction of the medusa jet on the background flow can be seen in the vertical direction at a distance 1.5d in the downstream.

Non-dimensional centerline velocity U/U_∞ vs. jet penetration ratio, defined as the ratio of vertical column height y to bell diameter d, for various medusae were plotted in **Fig. 7(III)**. Non-dimensional centerline velocity U/U_∞ is the ratio of medusa jet centerline velocity to ambient background flow velocity, i.e., 2 cm s^{-1}. From **Fig. 7(III)**, the jet penetration ratio y/d for a given U/U_∞ value looks larger for medusa with d = 2 cm. This figure also shows that at particular U/U_∞, jet penetration ratio decreased with increase in medusa bell diameter d. This decrease in penetration was due to the decrease in pulsation frequency with diameter from **Fig. 2(a)**. Thus an inverse proportionality relationship exists between jet penetration ratio and non-dimensional centerline velocity. We can observe the centerline velocity U of all medusa reached 90% of ambient velocity U_∞ at y = d. We can conclude the medusa jet affects the background flow for 1 d radially along the medusa central axis and in the downstream.

To better understand the deceleration zone as shown by LCS, average velocity and standard deviation at x/d= 1.5 was calculated for a fixed water column height of 60 mm. The standard deviation was more in the background flow for 2 cm medusa as shown in **Fig. 7(IV)** showing the evidence of medusa jet interaction with background flow with formation of deceleration zone which helps in feeding and capturing prey.

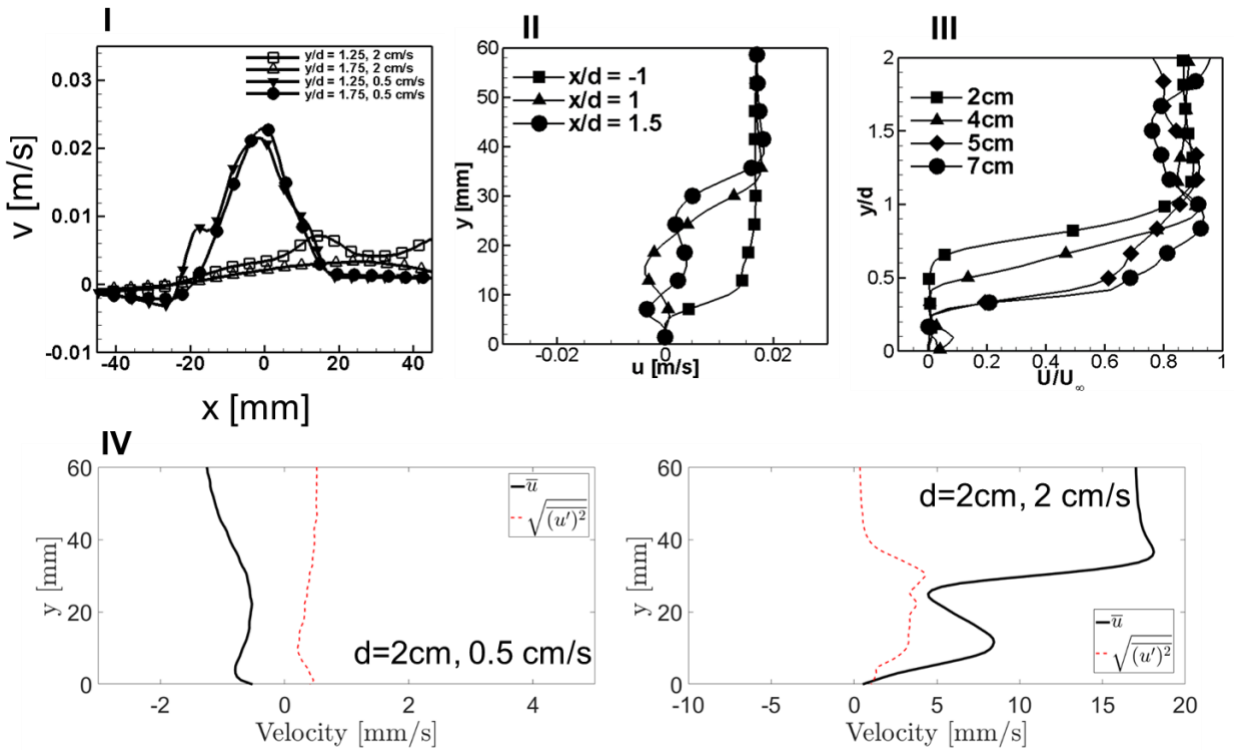

Figure 7. Medusa jet penetration characteristics. (I) vertical velocity profiles at 0.5 cm s^{-1} (solid markers) and at 2 cm s^{-1} (open markers). (II) Horizontal velocity component (u) was plotted against vertical height for 2 cm medusa at various positions along the substrate with background flow of 2 cm s^{-1}. (III) Non-dimensional centerline velocity, the ratio of centerline velocity (U) to ambient background flow velocity (U_∞ = 2 cm s^{-1}), was plotted against jet penetration along vertical height for various medusae with bell diameters 2 cm, 4 cm, 5 cm and 7 cm. (IV) Average velocity and standard deviation of horizontal velocity at x/d = 1.5 for bell diameter d = 2 cm at 0.5 cm s^{-1} and 2 cm s^{-1}.

Volumetric flux

Instantaneous volumetric flux was calculated at x/d = -0.5 and 0.5 for time resolved phase averaged up to y/d=2 vertically at each location as shown in **Fig. 8(I)**. Plots showed decreased in volumetric flux on the downstream during entire pulsing cycle compared to upstream during power stroke and recovery stroke, showing the presence of medusa and its pulsing mechanism influence with background flow.

Time averaged volumetric flux was calculated at x/d = -0.5,0.5 and 1 up to y/d = 2, for various bell diameters and different background flows (0.5 cm/s and 2 cm/s) as shown in **Fig. 8(II)**. Time averaged volumetric flux for 14 cycles at background flow 0.5 cm/s and 2 cm/s has similar trend with increase in bell diameter.

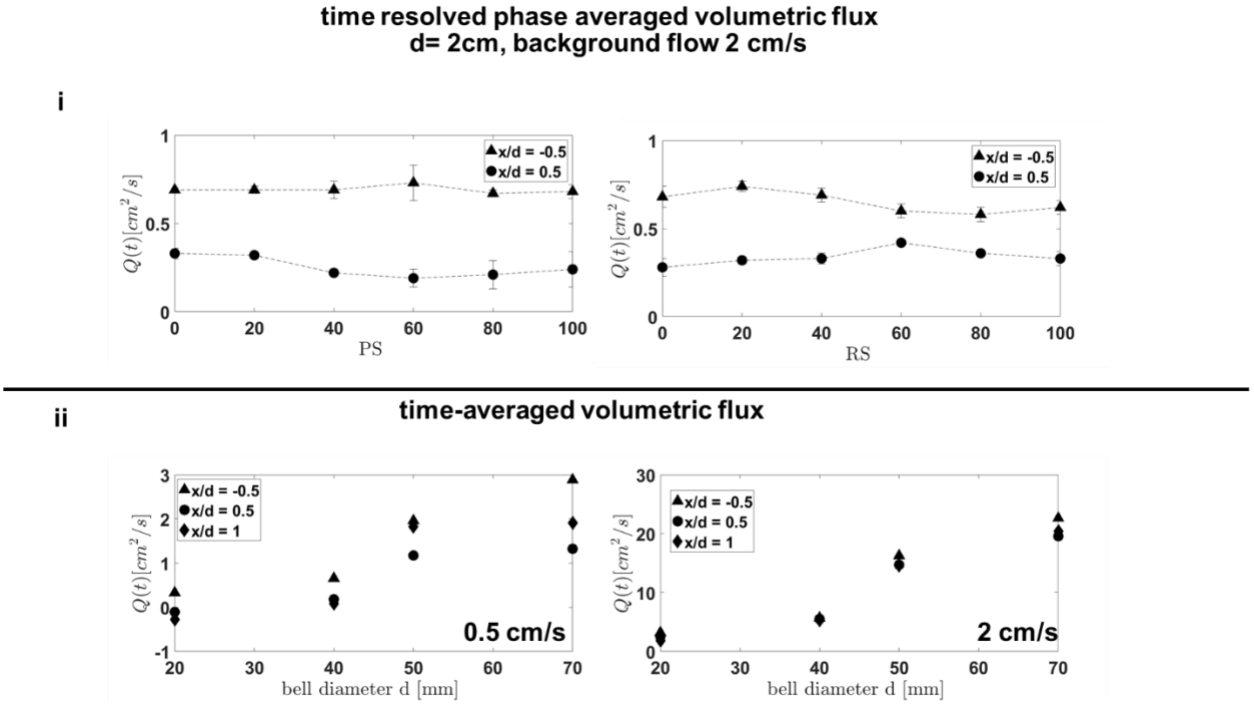

Figure 8.(I) Time resolved phase averaged volumetric flux per unit depth for medusa with bell diameter 2 cm, 2 cm s^{-1} background flow during A) power stroke (left top) and B) recovery stroke (right top). (II) time averaged volumetric flux values were plotted with change in diameters in background flow of 0.5 cm s^{-1} (left bottom) and 2 cm s^{-1}(right bottom)

DISCUSSION

Phase-averaged time-resolved velocity vector fields showed flow with peak velocities around 0.3 cm s^{-1} were generated during starting vortex formation in the power stroke. This starting vortex was pushed through the oral arms in the manner of a high-shear flow with magnitude roughly 0.3 cm s^{-1}. This value of peak velocities of the organismal currents remained same in both background flow conditions 0.5 cm s^{-1} and 2 cm s^{-1}. Thus when the background flow increases, the flow affects the medusa current and vice versa. The velocity vectors magnitude was slightly decreased in the upstream stream due to direct interaction of background flow, while in downstream, no significant changes were observed. Lack of change in velocity magnitudes downstream of the medusa was primarily due to the resistance or drag created by the individual bell pulsations. These results resemble engineering studies of jets in cross-flow (McFadden, 1986) such as the formation of asymmetric vortex rings. Thus more particulate matter can be entrained by suspension

feeding *Cassiopea* on the downstream side as compared to the upstream side, enabling timescales necessary for increasing capture and retention rates.

2D time-averaged far-field data showed a decrease in velocities with an increase in downstream location for each bell diameter. Also, calculations of centerline jet penetration for a background flow of 2 cm s^{-1} showed an inverse relationship between bell diameter and the corresponding centerline velocities. This decrease in penetration height with an increase in bell diameter is most likely caused by the decrease in pulsing frequency. Due to frequent pulsations by a smaller medusa, a larger cumulative effect can be realized via introducing vortices from multiple cycles into the background flow. Additionally, smaller medusa can generate more shear flow due to faster time scales of bell pulsation. Finally, qualitative flow visualization showed the breakup of large-scale vortices into small-scale flow structures due to the passage of flow generated in power stroke through the oral arms. This indicates that high resistance imposed by the oral arms plays a critical role in enhancing the suspension feeding mechanism, with or without background flow. Absolute mean volumetric flux was calculated with 2 cm s^{-1} background flow conditions to understand the flow entrainment along the medusa current. The smaller individuals had larger jet penetration, creating larger deceleration zone downstream and increasing time scale for sampling necessary for suspension feeding. In the case of large medusae, the absolute mean volumetric flux was increased showing a larger deceleration zone downstream of the organism when compared to smaller medusa. Such a large deceleration zone could be produced due to larger surface area and consequently larger form drag. This decelerated zone increases the time scale for suspension feeding, similar to what was described earlier for smaller individuals. The fundamental difference is the elevated role of the oral arm and body morphology in the case of larger medusa, whereas the faster rate of pulsations in smaller medusa results in increased jet penetration into background flow. Thus, individuals could alter their jet velocity by modulating their pulsing frequency based on the background flows, to increase the time scale for suspension feeding as shown in **Fig 9**.

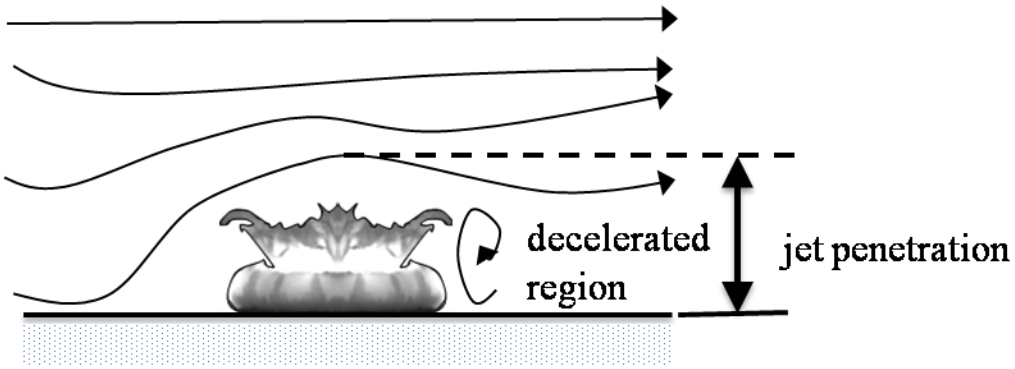

Figure 9. Formation of the decelerated zone in the downstream of medusa. For small medusa, the decelerated zone was formed due shear caused by its jet penetration in cross flow. For large medusa, the decelerated zone was formed due to form drag.

Particle capture by *Cassiopea* was not visualized or measured in this study. Measurements of *Cassiopea* feeding and retention rates are needed to understand the role of asymmetric vortex ring formation beneath the oral arms under non-zero background flow conditions. As these medusae live in fairly larger aggregations, it would be necessary to examine how individuals in a group interact when in the proximity of each other. This is especially necessary under non-zero background flow conditions. Previous experiments on corals showed that particle capture increased with increase in the number of neighbors under high background flow conditions, and decreased with increase in neighbors at low background flow conditions (McFadden, 1986). The pressure drop of 0.1 mm to 0.4 mm H_2O was found in sponges, cnidarians according to modern retention theory (Josrgensen, 1983). Since corals and *Cassiopea* spp. have same pressure drop range, whether *Cassiopea* would follow the same trend of particle retention as corals must be investigated. Though *Cassiopea* stays in patchy aggregations, it is unclear if there are synergistic interactions between neighbors. Modulating the pulsing frequencies based on nearest neighboring medusae as well as the background flow provides multiple pathways to tailor an individual's pulsations to maximize feeding success.

CONCLUSIONS

This paper provided details on how background flows interacts with the currents induced by *Cassiopea* medusa. *Cassiopea* pulsations locally alter the flow field up to a horizontal distance of around one diameter downstream from the medusa center. The cross-flow interaction with the upstream end of the bell margin resulted in an asymmetric starting vortex. Along the oral-aboral axis, the background flow reached 95% of its velocity at one diameter vertically measured from the substrate. The volumetric flux downstream of the

medusa decreased when compared to upstream position, due to the organism-induced jet interaction with background flow. The implications of the observed flow fields on suspension feeding were discussed.

List of symbols and abbreviations

d	bell diameter
F_i	fineness ratio
$\bar{Q}$	mean volumetric flux
Q_{max}	maximum volumetric flux
t	time
u	horizontal velocity
U	centerline velocity
U_∞	background/ambient velocity
v	vertical velocity
x	horizontal position
y	vertical position

REFERENCES

Adrian, R. J. (1991). Particle imaging techniques for experimental fluid mechanics. *Annu. Rev. Fluid Mech.* **23**, 261-304.

Arai, M. N. (1997). *Functional Biology of Scyphozoa*. London: Chapman & Hall.

Arai, M. N. (2001). Pelagic coelenterates and eutrophication: a review. *Hydrobiologia* **451**, 69-87.

Bajcar, T., Malačič, V., Malej, A. and Širok, B. (2009). Kinematic properties of the jellyfish Aurelia sp. *Hydrobiologia* **616**, 279-289.

Barker, J. C. (1983). Fluid mechanical aspects of suspension feeding. *Mar. Ecol. Pro. Ser.* **11**, 89-103.

Bartleson, R.D. (2004). Interactions of seagrass beds and the water column: effects of bed size and hydrodynamics. *Ph.D. thesis*, University of Maryland, College Park, MD, USA.

Bigelow, R. P. (1990). The anatomy and development of *Cassiopea* xamachana. *Boston Soc. Nat. Hist. Mem.* **5**, 191-236.

Blanquet, R. S., and Phelan, M. A. (1987). An unusual blue mesogleal protein from the mangrove jellyfish Cassiopea xamachana. *Mar. Biol.* **94**, 423-430.

Brotz, L., Cheung, W. W. L., Kleisner, K., Pakhomov, E., and Pauly, D. (2012). Increasing jellyfish populations: trends in Large Marine Ecosystems. *Hydrobiologia* **690**, 3–20.

Brusca, R. C. and Brusca, G. J. (2003). *Invertebrates*. Sinauer Associates,**23**, 974-976.

Colin, S. P., and Costello, J. H. (2003). In situ swimming and feeding behavior of eight co-occurring hydromedusae. *Mar. Ecol. Prog. Ser.* **253**, 305-309.

Costello, J. H., and Colin, S. (1995). Flow and Feeding by Swimming Scyphomedusae. *Mar. Biol.* **124**, 399-406

Costello, J. H., Colin, S. P., and Dabiri, J. O. (2008). Medusan Morphospace: Phylogenetic Constraints, Biomechanical Solutions, and Ecological Consequences. *Invertebr. Bio.* **127,** 265-290.

Crimaldi, J. P. (2008). Planar laser induced fluorescence in aqueous flows. *Exp. Fluids* **44**, 851-863.

Ferner, M. C., and Gaylord, Brian.(2008). Flexibility foils filter function: structural limitations on suspension feeding. *J. Exp. Bio*. **211**, 3563-3572.

Fleck, J. and Fitt, W. K. (1999). Degrading mangrove leaves of Rhizophora mangle Linne provide a natural cue for settlement and metamorphosis of the upside-down jellyfish *Cassiopea* xamachana Bigelow. *J. Exp. Mar. Bio. Eco.* **234**, 83-94.

Gordon, M. and Soria, J. (2002). PIV measurements of a zero-net-mass-flux jet in crossflow. *Exp. Fluids* **33**, 863-872.

Hamlet, C. L., and Miller, L. A. (2012).Feeding currents of the upside-down jellyfish in the presence of background flow. *Bull. Math. Biol.* **74**, 2547-2569.

Hamlet, C. L, Santhanakrishnan, A. and Miller, L. A. (2011). A numerical study of the effects of bell pulsation dynamics and oral arms on the exchange currents generated by the upside-down jellyfish *Cassiopea* xamachana. *J. Exp. Bio.* **214**, 1911-1921.

Huter, T.(1989). Suspension Feeding in Oscillating Flow: The Effect of Colony Morphology and Flow Regime on Plankton Capture by the Hydroid Obelia longissima. *Biol. Bull.* **176,** 41-49.

Jantzen, C., Wild, C., Rasheed, M., El-Zibdah, M., and Richter, C. (2010). Enhanced pore-water nutrient fluxes by the upside-down jellyfish *Cassiopea* sp. in a Red Sea coral reef. *Mar. Ecol. Prog. Ser.* **411**, 117-125.

Josrgensen, C. B. (1983). Fluid mechanical aspects of suspension feeding. *Mar. Ecol. Prog. Ser.* **11**, 89-10.

LaBarbera, M. (1984). Feeding currents and particle capture mechanisms in suspension feeding animals. *Amer. Zool*. **24**, 71-84.

Lipinski, D. and Mohseni, K. (2009). Flow structures and fluid transport for the hydromedusae *Sarsia tubulosa* and *Aequora victoria*. *J. Exp. Biol.* **212**, 2436-2447.

Lucas, C. H. (2001). Reproduction and life history strategies of the common jellyfish, Aurelia aurita, in relation to its ambient environment. *Hydrobiologia* **451**, 229–246.

Lukens, S., Yang, X., and Fauci, L. (2010). Using Lagrangian coheren structures to analyze fluid mixing by cilia. *Chaos* **20**, 017511.

Margason, R. J. (1993). Fifty Years of Jet in Cross Flow Research. Computational and Experimental Assessment of Jets in Cross Flow. AGARD-CP-534 Winchester, UK. NATO.

McFadden, C. S. (1986). Colony fission increases particle capture rates of a soft coral: Advantages of being a small colony. *J. Exp. Mar. Biol. Ecol.* **103**, 1-20.

Michael, L. (1984). Feeding currents and particle capture mechanisms in suspension feeding animals. *Amer. Zool.* **24**, 71-84.

Monismith, S. G., and Koscf, J. R. (1990). A study of model bivalve siphonal currents. *Limnol. Oceanogr.* **35**, 680-696.

Niggl, W. and Wild, C. (2010). Spatial distribution of the upside-down jellyfish *Cassiopea* sp. within fringing coral reef environments of the Northern Red Sea: implications for its life cycle. *Helgol. Mar. Res.* **64**, 281-287.

O'Riordan, C. A., Monismith, S. G., and Koseff, J. R. (1995). The effect of bivalve excurrent jet dynamics on mass transfer in a benthic boundary layer. *Limnol. Oceanogr*. **40**, 330-344.

Palomares, M. L. D. and Pauly, D. (2009). The growth of jellyfishes. *Hydrobiologia* **616**,11–21.

Peacock, T., and Dabiti, J. (2010). Introduction to focus issue : Lagrangian coherent structures.*Chaos* **20**, 017501.

Peng, J. and Dabiri, J. O. (2009). Transport of inertial particles by Lagrangian coherent structures: application to predator-prey interaction in jellyfish feeding. *J. Fluid Mech*. **623**, 75-84.

Pitt, K. A., Welsh, D. T., and Condon, D. H. (2009). Influence of jellyfish blooms on carbon, nitrogen and phosphorus cycling and plankton production. *Hydrobiologia* **616**, 133-149.

Purcell, J. E., and Arai, M. N. (2001)Interactions of pelagic cnidarians and ctenophores with fish: a review. *Hydrobiologia* **451**, 27-44.

Riisgård, H.U., Thomassen, S., Jakobsen, H., Weeks, J. M. and Larsen, P. S. (1993). Suspension-feeding in marine sponges halichondria-panicea and haliclona-urceolus-effects of temperature on filtration rate and energy- cost of pumping. *Mar. Ecol. Prog. Ser.* **96**, 177-188.

Santhanakrishnan, A., Dollinger, M., Hamlet, C. L., Colin, S. P., and Miller, L. A. (2012). Flow structure and transport characteristics of feeding and exchange currents. *J. Exp. Bio.* **215**, 2369-2381.

Shadden, S.C., Lekien, F., and Marsden, J.E. (2005). Definition and Properties of Lagrangian Coherent Structures. *Physica D: Nonlinear Phenomena* **212**, 271-304.

Shadden, S.C., Dabiri, J. O., and Marsden, J.E. (2006). Lagrange analysis of fluid transport in empirical vortex ring flows. *Physics of Fluids* **18**, 047105.

Taheri., A. (2018). Lagrangian coherent structure analysis of jellyfish swimming using immersed boundary FSI simulations. *J. Mech. Civil Engineering* **15**, 69-74.

Templeman, M. A. and Kingsford, M. J. (2010). Trace element accumulation in *Cassiopea* sp. (Scyphozoa) from urban marine environments in Australia. *Mar. Environ. Res.* **69**, 63-72.

Todd, B. D., Thornhill, D. J.and Fitt, W. K. (2006)Patterns of inorganic phosphate uptake in *Cassiopea* xamachana: A bioindicator species. *Mar. Pollut. Bull.* **52**, 515-521.

Welsh, D. T., Dunn, R. J. K., and Meziane, T. (2009).Oxygen and nutrient dynamics of the upside-down jellyfish (*Cassiopea* sp.) and its influence on benthic nutrient exchanges and primary production. *Hydrobiologia* **635**, 351-362.

Vogel, S. (1974). Current-induced flow through the sponge, Halichondria. *Biol. Bull.* **14,** 443-456.

Vogel, S. and LaBarbera, M. (1978). Simple Flow Tanks for Research and Teaching. *BioScience* **28**, 638-643.